J. Fluid Mech. (1971), *vol.* 46, *part* 2, *pp.* 299–319
Printed in Great Britain

Experiments on the instability of stratified shear flows: miscible fluids

By S. A. THORPE
National Institute of Oceanography, Wormley, Godalming, Surrey

(Received 12 June 1970)

Earlier papers have described a technique whereby a stratified shear flow may be produced under controlled conditions in the laboratory. A comparison between the experiments and theory is made here for small-amplitude unstable disturbances in an accelerating stratified free shear layer at the diffuse interface between layers of brine and water. In the early stages of the observed growth of the instability, which takes the form of growing waves, three measurable quantities can be compared with predicted values: the wavelength of the small amplitude waves, the time, which determines the flow conditions, and the growth rates of the waves. Some observations of the development of the disturbances to finite amplitude, the transition to turbulence and the resulting turbulence are reported.

1. Introduction

The study of the instability of stratified shear flows and the resulting turbulence is one of increasing practical and scientific importance. Shear instability has been identified as the cause of regular arrays of spiral rolls which are observed to form in the Mediterranean thermocline in association with internal waves (Woods 1968). In the atmosphere there is increasing evidence (see for example Browning & Watkins 1970) that such an instability is a main cause of clear-air turbulence above the troposphere and much effort is being made to predict and detect it. It seems probable that, as instruments are developed which can detect finer detail than has previously been possible, the occurrence of shear instability may be found to be widespread in the ocean and the atmosphere, in planetary atmospheres and in the solar photosphere, and it may prove to be a major limiting condition on large-scale currents.

We have already described a technique to produce a stratified shear flow in the laboratory. It was introduced in a paper published in 1968 (hereafter referred to as I), and in 1969 the development of instability at the interface between two immiscible fluids in shear flow was described (Thorpe 1969*a*, here referred to as II). Some preliminary results of an investigation of the instability at a diffuse interface between two miscible fluids in shear flow have been published (Thorpe 1969*b*, here referred to as III), and this study is now described in detail.

The majority of previous experiments on stratified shear flow instability have not provided suitably controlled conditions at the onset of instability. An

exception is the wind-tunnel experiment by Scotti & Corcos (1969). In this the initial spatial growth of waves was measured for very small wave slopes, much less than 0·1. The present experiments made with water and brine follow the development of instability up to large amplitudes and through a transition into turbulence. The qualitative details of this transition were the main subject of III.

The experiments are made in a long horizontal tube with almost square cross-section having perspex (plexiglass) sides and closed ends. It is completely filled with two layers of fluid – the upper water and the lower brine – which is usually coloured with dye so as to make it distinguishable from the water. (A few experiments with more than two layers are reported in § 3.) The density profile is varied by allowing diffusion to occur for different lengths of time. When the tube is suddenly tilted through a small angle, θ, a uniformly accelerating shear flow is initiated in the centre of the tube and this becomes unstable after a few seconds. The growth of instabilities is shown in figure 1 (plate 1), and is recorded by cameras in the experiments. The analysis and interpretation of the data collected in this way is the subject of this paper.

The theoretical background is discussed in § 2. The nature of the accelerating flow can be predicted from a knowledge of the initial density profile, as was shown in I. The problem of extending Squire's theorem to an accelerating flow is considered, and use is made of a quasi-steady approximation to estimate the rate of growth of disturbances. This approximation has already been used and tested against an exact solution for immiscible fluids in II. Some numerical studies of steady inviscid flows with error function and hyperbolic tangent function density and velocity profiles have been made (Hazel 1970) and these are reviewed in § 2.4 and, in § 2.5, are applied to predict the way in which disturbances will grow in the accelerating flow of the experiments. The presence of viscosity reduces the velocity gradients in the shear region at the diffuse interface between the water and brine and this can be accounted for, but not enough is yet known about the effect which viscosity has upon the growth rates of the unstable disturbances. There is, however, evidence from the experiments and the theory of homogeneous free shear layers that, at the Reynolds numbers appropriate to the present experiments, the effect of viscosity is not very great.

The experiments are described and the results compared with theoretical predictions in § 3. The small-amplitude inviscid theory appears to predict some features of the growth of the disturbances quite well, even though the disturbance amplitude is appreciable at the earliest times at which it can be measured. In particular the orientation and wavelength of the disturbances are well estimated. There is considerable scatter in the observed growth rates which are mostly less than those predicted. The initial 'noise level' in the tube is unknown and, as was found in II, this produces some difficulties in the interpretation of the results. The growth of the disturbances is described in § 3.3 up to the onset of small-scale irregularities in the flow, and some features of the developing turbulent flow are reported in § 3.4.

2. Theory

2.1. *The accelerating flow*

We consider the motion of a stably stratified fluid from a state of rest between parallel planes, $z = \pm \frac{1}{2}H$, inclined at an angle θ to the horizontal. The effect of the lateral walls will be ignored and the x axis is taken parallel to the planes up the line of greatest slope, and the z axis upwards (as in figure 1 in I). The density of the fluid, ρ, is supposed to depend on co-ordinate z alone when the fluid is initially at rest. In the accelerating flow which ensues, the velocity $(u, 0, 0)$ is parallel to the boundaries and, as was shown in I,

$$u(z,t) = gt\sin\theta\left(\frac{H}{\rho(z)\int_{-\frac{1}{2}H}^{\frac{1}{2}H}\frac{dz}{\rho}} - 1\right), \tag{1}$$

if viscosity can be neglected. (The effect of viscosity will be examined in § 2.6.) If $\rho = \rho_0(1-\Delta f(z))$, where ρ_0, Δ are constants, $\Delta \ll 1$ and $f(z) = -f(-z)$ is of order unity, then approximately

$$u = g\Delta f(z)\, t\sin\theta \tag{2}$$

in the accelerating flow.

In the experiments, the density profile is produced by allowing diffusion to occur for a time τ across an initially sharp interface separating two homogeneous layers of brine and water of equal depth. The resulting density distribution in the tube is

$$\rho = \rho_0[1-\Delta\,\mathrm{erf}\,(z/2(\kappa\tau)^{\frac{1}{2}})], \tag{3}$$

provided that $H/4(\kappa\tau)^{\frac{1}{2}} \gg 1$—that is, diffusion from the parallel planes is negligible—and where initially the upper fluid (water) has uniform density $\rho_0(1-\Delta)$ and the lower fluid (brine) has a uniform density $\rho_0(1+\Delta)$, and κ is the molecular diffusivity of salt in water.

If $\Delta \ll 1$ and $t \ll \tau$, the resulting velocity distribution at a time t after the tube has been tilted is approximately

$$u = g\Delta\,\mathrm{erf}\,(z/2(\kappa\tau)^{\frac{1}{2}})\, t\sin\theta. \tag{4}$$

This, and its derivatives, provide a good approximation in the experiments, in which $\Delta < 0{\cdot}09$, $t/\tau < 0{\cdot}01$.

2.2. *The disturbed flow*

For a steady two-dimensional inviscid shear flow Yih (1955) has extended Squire's theorem and has shown that for each infinitesimal three-dimensional wave making an angle ϕ with the basic flow, there is an infinitesimal two-dimensional wave having the same growth rate but with characteristic Richardson number increased by a factor $[1/\cos^2\phi]$. In the study of two-dimensional disturbances to stratified shear flows it is usually found that an increase in Richardson number reduces the growth rate of unstable waves and, in these flows, the most unstable wave disturbances will therefore be two-dimensional. The inverse relation between Richardson number and growth rate is expected intuitively since an increase in Richardson number represents an increase in static stability arising

from buoyancy forces in the increased density gradients, but such a relation does not always hold true. Thorpe (1969*c*) has found a flow which is destabilized by the presence of (statically stable) density gradients, and Miles (1963, see figure 2) has found a flow which (for wave-numbers between 1 and 2) becomes unstable as the characteristic Richardson number is increased. It does not follow therefore that two-dimensional disturbances are *always* the most unstable, and some caution is needed. It has been found, however, that in a few experiments we have made in which instability has been observed to develop on a *steady* flow with error function profiles (profiles given by (2) and (3) but with t having a constant value) the disturbance has a two-dimensional nature when it is of sufficient amplitude to be observed (wave slopes of about 0·01; see figure 2 of III) and the two-dimensional character continues until the disturbance is very large. The two-dimensional nature of the small amplitude disturbances is expected since, for the appropriate density and velocity profiles, the growth rates decrease with increased characteristic Richardson number (Hazel 1970; see § 2.4 below), but the ensuing two-dimensional flow at large wave-amplitude has not been predicted and deserves study. Drazin's (1970) study of finite-amplitude disturbances when the flow is just unstable is not applicable to the present experiments for, as will be seen, the instability is first observed when the Richardson number, which provides the criterion for instability, is well below critical.

We now consider the nature of a disturbance in the accelerating flow produced in the experiments, and suppose that a space-wise periodic disturbance to the accelerating flow given by (2) is directed at an angle ϕ to the x axis. Let us now take new axes (x', y', z), where x' is in the direction of the disturbance and so no variation of phase of the disturbance occurs in the y' direction. If

$$[u(z,t),\, v(z,t),\, w(z,t)]\, e^{ikx'}$$

is the disturbance velocity measured in these new co-ordinates, and $\rho' e^{ikx'}$ and $p' e^{ikx'}$ the disturbed density and pressure respectively, the linearized equations of motion become

$$\frac{\partial u}{\partial t} + ftg\Delta \sin\theta \cos\phi iku + wtg\Delta \sin\theta \cos\phi f' = -\frac{1}{\rho_0} ikp' - \frac{g\rho'}{\rho_0} \sin\theta \cos\phi, \tag{5}$$

$$\frac{\partial v}{\partial t} + ftg\Delta \sin\theta \cos\phi\, ikv + wtg\Delta \sin\theta \sin\phi f' = -\frac{g\rho'}{\rho_0} \sin\theta \sin\phi, \tag{6}$$

$$\frac{\partial w}{\partial t} + ftg\Delta \sin\theta \cos\phi\, ikw = -\frac{1}{\rho_0} \frac{\partial p'}{\partial z} - \frac{g\rho'}{\rho_0} \cos\theta, \tag{7}$$

$$\frac{\partial \rho'}{\partial t} + ftg\Delta \sin\theta \cos\phi\, ik\rho' + w\Delta\rho_0 f' = 0, \tag{8}$$

$$iku + \frac{\partial w}{\partial z} = 0, \tag{9}$$

where the Boussinesq approximation has been made, $f' \equiv df/dz$, k is the wave-number, and viscosity and molecular diffusivity are neglected.

For small values of θ, $\cos\theta$ is approximately unity and (5), (7), (8) and (9)

depend on $\sin\theta$ only. They are identical to the set of equations for a two-dimensional disturbance† in a fluid with the same density profile but contained in a tube tilted through a smaller angle, $\theta\cos\phi$. The behaviour of three-dimensional disturbances can thus be modelled by two-dimensional ones. Moreover, if the fluid is such that a two-dimensional disturbance will grow by a given factor (say 100 times its initial amplitude) more rapidly as the angle of tilt is increased, then of all the disturbances which can occur the first to grow by this factor will be two-dimensional. An example of this property was found in II. When a tube containing two immiscible fluids was tilted it was found that the time taken for a two-dimensional disturbance to increase its amplitude by a given factor was reduced if the angle of tilt was increased. If initially all the possible disturbances had the same amplitude independent of their orientation, then two-dimensional disturbances would subsequently be the largest in the unstable motion. (The result was proved in that case for all angles of tilt.) We shall consider in § 2.5 whether fluids with density profiles of the form (3) considered here have the property. It is, however, plausible that they may, since the Richardson number of the flow (see I) is

$$R_i = \frac{\cos\theta}{N^2t^2\sin^2\theta} = \frac{\cos\theta(\pi\kappa\tau)^{\frac{1}{2}}\exp(-z^2/4\kappa\tau)}{\Delta g t^2\sin^2\theta} \tag{10}$$

(where N is the Brunt–Väisälä frequency), and this is increased as θ decreases at given times t and τ and at each position z.

When θ is not small, a term $\cos\theta$ appears in (7) and the equations are no longer equivalent to those of a two-dimensional disturbance. In the experiments the angle of tilt is small (less than 11°).

2.3. *The quasi-steady approximation*

We shall call the quasi-steady approximation that in which the growth rate of an unstable disturbance at a given time t in the accelerating flow is supposed to be the same as it would be in a steady flow, with the same distribution of density and velocity as the accelerating flow has at that instant of time. In the investigation II of the instability of two immiscible fluids in shear flow it was shown by direct comparison between an exact solution and that developed on the basis of a quasi-steady approximation that the latter was a very good approximation. The time at which a two-dimensional disturbance would have increased its amplitude by a given proportion was well predicted and the growth rates were also well predicted except when growth first occurred. In general, the approximation will be valid provided that the disturbances are small (the maximum slope of lines of constant density must be small) and the rate of change of the accelerating flow ($[\partial u/\partial t]/u = 1/t$) is much less than the growth rate of the disturbance given by the quasi-steady approximation. This approximation will not therefore be valid when it predicts very small growth rates—that is, near conditions of marginal stability for a steady flow. Fortunately the experiments are such that we are not concerned with this region, but rather that in which the steady-flow

† By a two-dimensional disturbance we mean one in which the wave-number is directed in the direction of flow.

theory predicts unstable conditions with large growth rates, and the quasi-steady approximation appears to be justified. We shall therefore consider the results available from the theories of the instability of steady shear flows.

2.4. *Solutions for steady flows*

The literature on the instability of steady stratified shear flows is extensive and we shall not attempt to survey it here. Drazin & Howard (1966) have recently reviewed the subject. The main results stem from solutions of the Taylor–Goldstein equation (Thorpe 1969*c*). Numerical solutions have recently been obtained for a variety of density and steady velocity profiles by Mr Philip Hazel of Cambridge University (Hazel 1970) and I am indebted to him for examining

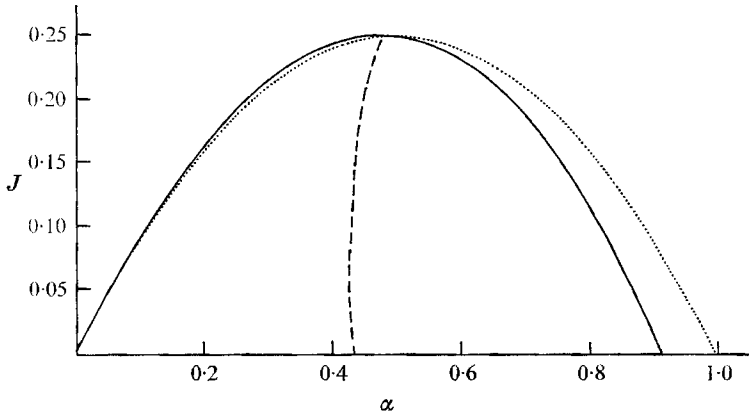

FIGURE 2. The neutral curve for density and velocity profiles of equation (11) (full line), the curve of maximum growth rate (dashed), and the curve $J = \alpha(1-\alpha)$.

some particular profiles which are relevant to the experiments. Figure 2 shows the neutral curve (α, J) for the non-dimensional profiles

$$u = F(z), \quad \rho = 1-(J/g)F(z) \quad (F(z) = \operatorname{erf}(z\pi^{\frac{1}{2}}/2)) \tag{11}$$

in an infinite fluid, and the curve of the maximum growth rate in the unstable region. J is defined as the minimum Richardson number, which occurs at $z = 0$ and α is the wave-number of the disturbance. The waves which grow most rapidly have wave-numbers below the wave-number which first becomes unstable as the Richardson number decreases. All the eigensolutions found were stationary. Table 1 shows the non-dimensional growth rates of unstable disturbances of wave-numbers $\alpha = 0{\cdot}40$, $0{\cdot}44$. Also shown in figure 2 is the neutral curve for $F(z) = \tanh z$ found by Holmboe (1962; $J = \alpha(1-\alpha)$). The two neutral curves are very similar except near $\alpha = 1$. The growth rates were also found to be similar.

The effect of the presence of horizontal boundaries has also been examined, although only for $F(z) = \tanh z$. The effect of decreasing the distance between the horizontal plane boundaries at $z = \pm \frac{1}{2}h$ (h is non-dimensionalized with respect to the thickness of the transition region at $z = 0$) is first to destabilize the longer

wavelengths and then to stabilize all wavelengths; as h takes successively smaller values, the neutral curve at small α rises until approximately $h = 5$ and then further decrease of h causes a collapse of the neutral curve towards small wave-numbers at $J = 0$. The wave-number of the waves which first become unstable as the Richardson number decreases (the critical wave-number) is not much affected until h is less than 10. The effect on the growth rates of decreasing h is

Wave-number α	Richardson number (J)	Growth rate (αc_i)
0·40	0·20	0·0446
0·40	0·15	0·0885
0·40	0·10	0·1264
0·40	0·05	0·1602
0·40	0·01	0·1848
0·44	0·20	0·0474
0·44	0·15	0·0896
0·44	0·10	0·1270
0·44	0·05	0·1606
0·44	0·01	0·1855

TABLE 1. The growth rates for the error function profiles of density and velocity, equation (11)

not known, but the general changes suggest that the curve of maximum growth rate will be displaced towards the small wave-numbers, the effect becoming significant at about $h = 10$. (In dimensional terms this corresponds to

$$H = 10(\pi\kappa\tau)^{\frac{1}{2}}$$

for the error function profile of the experiments.)

Hazel has also considered the effect of different length-scales in the profiles of velocity and density. R is the ratio of the velocity length-scale to the density length-scale in the profiles

$$u = R\tanh(z/R), \quad \rho = 1-(J/g)\tanh z.$$

For $1 < R < \sqrt{2}$, J is the minimum Richardson number in the flow and the neutral curve is the stability boundary. The unstable waves are also stationary, and the critical wave-number non-dimensionalized with respect to the density length-scale, α_c, is found to correspond to $J = \frac{1}{4}$. Near $R = 1$,

$$\alpha_c = (0{\cdot}7/R) - 0{\cdot}2, \tag{12}$$

approximately (Hazel has actually non-dimensionalized with respect to the velocity length-scale). We shall show in § 2.6 that viscosity has the effect of increasing the length-scale of the velocity transition region. At the onset of the observed instability in the experiments the value of R is between 1 and 1·34 and in this range the percentage variation in the critical wave-number from (12) may be as much as 35 %. In the majority of experiments the value of R is between 1 and 1·1 (corresponding to 13 % variation) and, in any case, R is not steady during the early growth of the waves. The effect of the different length-scales,

like that of the boundaries at finite distance and the position of the maximum growth-rate curve (figure 2), is to favour wave-numbers which are less than the critical wave-number, 0·48, of the error function profiles (11) in an infinite fluid. The effect of the different length-scale on the growth-rates of unstable waves has not been considered in great detail, but Hazel's available results indicate that near $R = 1$ the changes produced are quite small.

2.5. *The predicted growth curves*

Using the quasi-steady approximation we can now predict the way in which the amplitude of a two-dimensional disturbance of a given wave-number will vary with time in the accelerating flow. The effects of viscosity and the presence of the walls of the apparatus will be neglected. For each wave-number, α, a cubic expression in J has been estimated which fits the non-dimensional growth-rates of table 1. The dimensional growth-rates are then found by multiplying by the reciprocal of the appropriate time scale, $[U/L]$. Here U is taken as $g\Delta t \sin\theta$, to which u, given by (4), tends as z tends to infinity; L is $(\pi\kappa\tau)^{\frac{1}{2}}$, which measures the thickness of the transition region near $z = 0$. In the accelerating flow the minimum Richardson number, J, varies as $1/t^2$ (see (10)), and its value is substituted into the expression for the dimensional growth-rate. For example, for the non-dimensional wave-number $\alpha = 0{\cdot}44$ (which is near the curve of maximum growth-rate of figure 2 for the error function profiles) we find

$$\frac{1}{a}\frac{da}{ds} = \frac{s}{\tan\theta}\left\{0{\cdot}772 - \frac{0{\cdot}599}{s^2} - \frac{0{\cdot}069}{s^4} - \frac{0{\cdot}104}{s^6}\right\}, \tag{13}$$

where a is the amplitude of the disturbance, and

$$s = \frac{t\sin\theta[0{\cdot}248g\Delta]^{\frac{1}{2}}}{[\pi\kappa\tau\cos^2\theta]^{\frac{1}{4}}}.$$

(s is chosen so that $J = 0{\cdot}248/s^2$, and for this wave-number the growth-rate is zero for $J = 0{\cdot}248$ at $s = 1$.)

Integrating (13) we find

$$\frac{a}{a_0} = \left(\frac{1}{s}\right)^{0{\cdot}599/\tan\theta} \exp\left\{\frac{s^2-1}{\tan\theta}\left[0{\cdot}386 - \frac{0{\cdot}060}{s^2} - \frac{0{\cdot}026}{s^4}\right]\right\}, \tag{14}$$

where a_0 is the amplitude of the disturbance when it first begins to grow; that is, at $J = 0{\cdot}248$. For small values of $(s-1)$, near marginal stability in the steady flow, (13) is a poor approximation as remarked in § 2.3, for the predicted growth rates are very small, but it rapidly improves. For $s > 1{\cdot}48$ (14) appears to be a very good approximation since the growth rates exceed $1/t$ by a factor of $1/2\tan\theta$ (which is large for the small θ of the experiments) or more, and at such times the amplitude is unlikely to be much affected by the effect of inaccuracies in the predictions of growth rate whilst the latter were small. When $s = 1{\cdot}48$, $J = 0{\cdot}114$, and so for some θ the approximation will not be valid until the Richardson number is quite small.

Expressions similar to (13), (14) may be found for other wave-numbers. Figure 3 shows the variation of $\tan\theta \log_e(a/a_0)$ with $1/2J^{\frac{1}{2}}$, derived for $\alpha = 0{\cdot}44$ from (14),

and for $\alpha = 0{\cdot}40$. The term $1/2J^{\frac{1}{2}}$ is proportional to t and so figure 3 shows the growth of a disturbance with time. The close proximity of the curves for $\alpha = 0{\cdot}40$ and $\alpha = 0{\cdot}44$ indicates that these wave-numbers will grow at almost the same time. It is therefore to be expected that in the experiments some scatter in the wave-numbers which are first observed to grow will be found, since a band of wave-numbers grow almost simultaneously. If $\tan\theta = 0{\cdot}1$ (a value typical of the experiments), then 100-fold growth will have occurred when $J = 0{\cdot}077$. For smaller angles of tilt, 100-fold growth will occur at larger values of J. Also shown in figure 3 are some experimental points to which reference will be made in § 3.2.

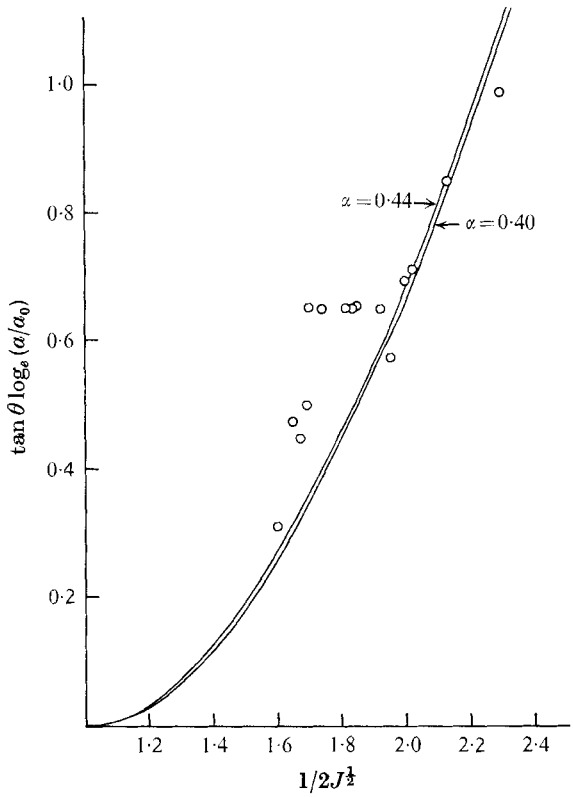

FIGURE 3. The predicted variation of $\tan\theta \log_e (a/a_0)$ with $1/2J^{\frac{1}{2}}$ for $\alpha = 0{\cdot}40$ and $\alpha = 0{\cdot}44$, with experimental points for $\log_e (a/a_0) = 6$ and wave-slope of 0·2.

Differentiation of (14) (and similar expressions for other values of α) with respect to θ at a fixed time t shows that a/a_0 increases with θ. From the remarks in § 2.2 it is therefore expected that the waves which will first be observed to grow in the experiments will be two-dimensional, unless the initial 'noise' distribution strongly favours three-dimensional waves, or some non-linear or viscous effects are important when the waves are very small or unless the quasi-steady approximation is very poor in the region in which there is doubt about its validity. The results presented in II indicate that the latter possibility is unlikely.

2.6. *The effect of viscosity on the accelerating flow*

So far it has been assumed that the accelerating flow is inviscid, and we now consider the effect of viscosity. In I it was shown that a Laplace transform technique may be used to find the velocity profile in an accelerating flow with a constant coefficient of viscosity μ. The viscosity is not constant in the experiments and may vary by as much as 30 %, but a constant viscosity model will give a useful approximation. The details of the calculations are given in the appendix. It is shown there that for flows resulting from the density profile (3), the ratio of the velocity gradient at $z = 0$ in a viscous flow to that at $z = 0$ in an inviscid flow is

$$Q = \frac{2}{\{1+[1+(4/\pi)\,(\nu t/\kappa\tau)]^{\frac{1}{2}}\}}, \tag{15}$$

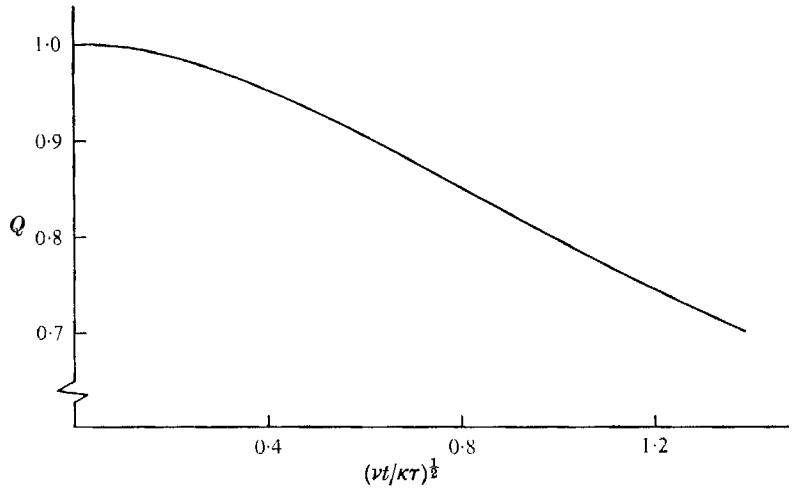

FIGURE 4. The variation Q with $(\nu t/\kappa\tau)^{\frac{1}{2}}$.

where $\nu = \mu/\rho_0$. The parameter Q may be regarded as the ratio of a length-scale characterizing the region of density variation to that characterizing the region of velocity variation in a viscous flow. Figure 4 shows the variation of Q with $(\nu t/\kappa\tau)^{\frac{1}{2}}$. The choice of an error function profile in density is seen to be fortunate since initially Q varies very slowly with $(\nu t/\kappa\tau)^{\frac{1}{2}}$, a parameter which may be identified as the ratio of a viscous length-scale to the diffusion length-scale.

In presenting the results of the experiments and in comparing them with the available theory, the effects of viscosity will be accounted for in three ways. Viscosity makes the shear at $z = 0$ smaller than that estimated by the inviscid theory by a factor Q. The Richardson number of the flow is thus increased by $1/Q^2$. The growth-rates are non-dimensionalized with respect to the shear at $z = 0$; the shear is decreased and thus the non-dimensional growth-rates estimated from the observations should be increased by a factor $1/Q$ to make them comparable with those predicted. The effect of viscosity produces different length-scales as remarked in § 2.4; in an inviscid flow the density and velocity have the

same length-scales, but in the viscous flow the velocity has a length-scale greater by $1/Q$, and the critical dimensionless wave-numbers are reduced by virtue of result (12).

The curves of figure 3 are valid only for strictly inviscid flows. It appears to be of little practical value to attempt to correct these, however, particularly as the influence of viscosity on the growth-rates of the waves is not precisely known.

It seems likely that, beyond its influence on the mean velocity profile, viscosity has little effect on the conditions at the onset of instability at Reynolds numbers greater than about 100. Esch (1957) has shown that in an unstratified shear flow the neutral curves are not much affected by viscosity at wave-numbers for which the product of the Reynolds number and the non-dimensionalized wave-number is greater than 100. Betchov & Szewczyk (1963) have examined the effect of viscosity on the growth rates in a hyperbolic tangent shear layer at Reynolds numbers of 40 and less, and their results suggest that at Reynolds numbers of about 100, the growth rates in a viscous flow will not differ significantly from those in an inviscid flow. Freymuth (1966) found in his experimental studies of a shear layer (again unstratified) that the early stages of the growth of unstable waves were not affected by changes in the Reynolds number, R_e (based on the momentum thickness of the layer) in the range

$$61 < R_e < 334.$$

It is probable that similar results may hold for a stratified shear flow. Without modification, the present experiments are not suitable to test this conjecture.

3. Experiments and comparison with theory

3.1. *General description*

The apparatus is a tube with internal dimensions 487·5 cm in length, 10 cm in height and 10·25 cm in width. The top and bottom are made of machined aluminium channel sections and the front and rear sides are of $\frac{1}{2}$ in. thick perspex. The ends are made of aluminium. One end is fitted with inlet and draining tubes and a plate which arrests the inflow to reduce mixing in filling. The other end has a tapered slot fitted to it which leads into a tube, and this is arranged to allow the removal of bubbles of air when the tube is being filled. The tube is braced by a support system to prevent sagging and the sag along the length of the tube in the experiments is less than 3 mm. It is free to pivot about a horizontal axis which is at right angles to the tube and which is at a distance of 12·5 cm below its centre.

The water used to fill the tube is left to stand for some time, usually 48 h, to remove air bubbles, before it is run into the tube from a constant head apparatus. The tube is filled in an inclined position at about 45° to the horizontal. The fresh water is first run in from the lower end and the brine solution (coloured with potassium permanganate in most of the experiments) is slowly run in under the water, forcing the water up the tube and eventually all the air out of the tube through the upper end-plate. Filling is continued until the interface between the water and the brine, which can be seen either because the brine is dyed or

through the refraction effects associated with the interface, reaches the centre of the tube. The interface is usually quite clear and sharp if care is taken when the first brine is introduced. Filling usually takes about 1 h and the thickness of the interface, judged by eye, is about 1 cm when filling is complete. Taps at the ends are then closed and the tube is slowly tilted by hand into a horizontal position. With experience this can be done in about 8 min with very little sign of mixing. The area of the interface is considerably increased in this tilting (by a factor of about 22), and the density gradients at the interface are considerably increased.

The tube is left in a horizontal position for a time to allow diffusion to occur at the interface. During this time photographs are taken of a bar inclined at about 45° to the horizontal which is viewed through the tank. The gradients of refractive index at the interface produce a distorted image of the rule (Mowbray 1966) and the photographs are used to obtain an estimate of the equivalent total diffusion time, τ, the time which elapses between the tube reaching a horizontal position and the experiment being made plus a correction representing the time necessary for diffusion to produce the gradients at the interface at the moment when the tube reaches the horizontal position. The correction (usually about 14 min but sometimes larger) is obtained by plotting the square root of the length of the rod which is distorted by interface, against time; the negative intercept on the time axis is taken as the correction. This method is only approximate, but for most experiments the correction is small compared to τ, and, as τ itself appears in the theory to some small fractional power, the errors are not serious.

When the time to make the experiment arrives, two cameras are started and a second or so later the tube is rapidly tilted through a small angle, θ. The time taken to tilt the tube is usually between $\frac{1}{4}$ and $\frac{1}{3}$ sec. A 35 mm Nikon camera, fitted with a motor drive to take about 3 frames/sec, photographs about 140 cm of the central length of the tube, and the photographs are used to determine the wavelength of the eventual instability. The second camera is a 16 mm Bolex which is operated at between 40 and 78 frames/sec, depending on the expected rapidity of the wave growth. (The speeds were checked by filming a stop watch.) The colour ciné film shows about 80 cm of the tube and is used to record the time at which the tube is tilted and the subsequent growth of instability.

In the majority of the experiments, Δ, the fractional density difference between the fluids, was about 0·085. In experiments made with smaller density differences the instability was found to occur only after a time at which viscosity was important (Q is appreciably less than 1), unless large tilt angles were used. These were avoided so that the time to tilt the tube was kept small. The time of events in the accelerating flow, t, was measured as the time from the moment at which the tube reached its maximum inclination plus half the time taken to tilt the tube.

The growth of the instability, which looks at one stage (*c*) very like the decorative patterns sometimes found on Roman mosaic pavements, is shown in figure 1 (plate 1). The transition from waves into spiral rolls and then into turbulence has been described already in I and III. The growth is remarkably regular and well organized; patches of about five waves or more can frequently

be seen in which a very regular wavelength is maintained and in which the waves grow at the same time. Instability occurs at about the same time all along the central portion of the tube, indicating a very rapid growth at this time. In the experiments with two layers of equal depth the instability appears to be stationary. The two-dimensional nature of the instability is demonstrated on figure 5 (plate 2), which are negatives taken from the ciné film of instability in a tube made entirely of perspex which was described in I. A thin layer of dye (this appears as white streaks) has been injected at the interface. The lower part of the photographs show the tube viewed directly from the side and the upper part shows a view from above which is reflected through a mirror. The photographs demonstrate the way in which fluid near the interface is redistributed as the waves grow (see also III). There is a clear similarity between this instability and that observed by Woods (1968, see figure 9).

Precise measurements of the wave amplitude during the early stages of growth are not possible, for the dye in the lower, brine, layer has diffused about as much as the brine and the interface is not sharp. However, the interface soon becomes very sharp because of the redistribution of fluid at the interface, and, at wave slopes greater than about 0·2, it is easy to measure the wave amplitude from the photographs. The wave slope is defined here as half the total crest-to-trough amplitude of the disturbance, times the wave-number. Wave slopes of 0·2 are the first at which it is possible to estimate the growth rate of the disturbance.

The molecular diffusivity of sodium chloride in water, κ, is taken as

$$1{\cdot}40 \times 10^{-5}\,\mathrm{cm^2\,sec^{-1}}$$

in the estimation of the diffusion at the interface in the experiments and the kinematic viscosity of the fluids, ν, is taken as $1{\cdot}00 \times 10^{-2}\,\mathrm{cm^2\,sec^{-1}}$. No account of the variations arising from either temperature changes or differing concentrations of brine have been made.

3.2. *The early stages of instability*

It is to be expected on theoretical grounds (§ 2.5) that the minimum Richardson number in the flow, J, will be much less than the critical value of 0·25, estimated for steady flows, when instability is first observed in the accelerating flow of the experiments. This is indeed found. Some effort was made to measure the time t, and thus to estimate J, at the onset of instability, but the precise moment of instability was thought to be rather subjective and, instead, the values of J at wave slopes of 0·2 have been estimated and are plotted in figure 3 with a choice of $a/a_0 = 403$ ($= \exp 6$), to give a good fit. (The onset of instability was first observed at values of J about 20 % larger.) The corresponding slope of the presumed initial disturbance at $J = 0{\cdot}25$ is approximately 5×10^{-4}, which does not seem to give an unreasonable estimate for the probable initial noise-level in the tube. This noise may arise in a number of ways. Brownian movement, the vibration in the fluid and structures of the tube caused by the initial acceleration and deceleration whilst the tube is being tilted, vibrations of the floor and vibrations in the air surrounding the tube, may all contribute. Without knowledge

of the initial disturbances, the selection of a/a_0 cannot be justified. The repeatability of the experiments which was remarked on in I seems, however, to support the assumption that the noise level is fairly constant from one experiment to another. Although the wave slope of 0·2 is probably beyond the range of linear theory (and the redistribution of fluid in the interface suggests this) the general fit of the experimental points to the theoretical is encouraging. The values of J (and therefore s, see § 2.5) are such that the quasi-steady approximation is a good approximation to the theoretical growth rates, we therefore compare the observed growth rates with those predicted by the approximation.

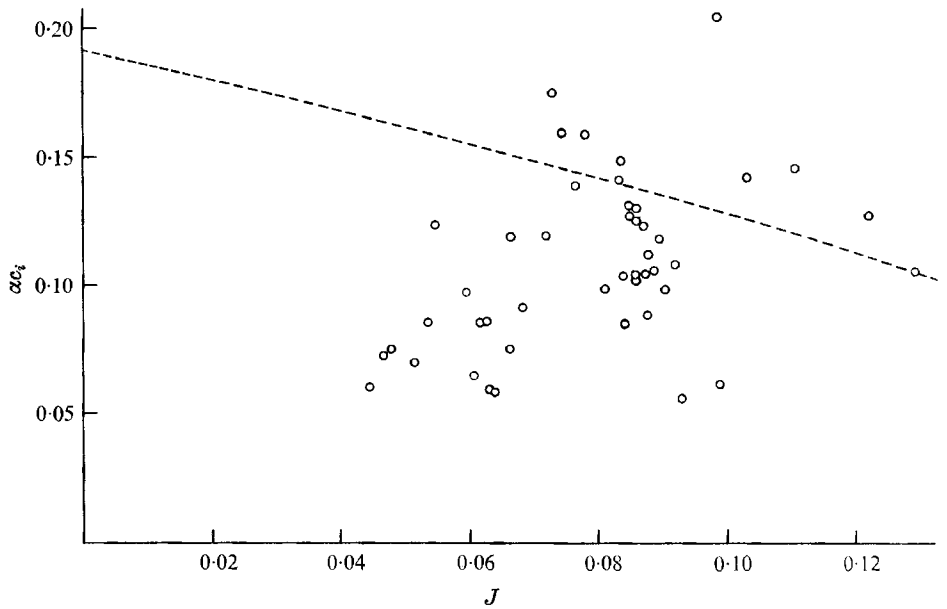

FIGURE 6. The observed non-dimensional growth rates, αc_i, as functions of the minimum Richardson number, J, when the slope of the disturbance is 0·2. The dotted line indicates the predicted growth rates for infinitesimal disturbances of wave-number $\alpha = 0{\cdot}44$.

The growth rates of the instability, αc_i, non-dimensionalized with respect to the shear at the interface at wave slopes of 0·2, are plotted against J in figure 6. The growth rates have been found from the ciné film by measuring the crest-to-trough amplitudes of individual waves, plotting their variation with time and estimating the growth rates from the plotted curves. The dotted line in figure 6 is the theoretical curve of the growth rates of infinitesimal disturbances of wave-number $\alpha = 0{\cdot}44$ computed by Hazel for the error function profile (table 1) and which have been assumed in the quasi-steady approximation. There is considerable scatter in the experimental points arising both from the method of measuring the growth rates and from real variations between individual waves. In general, the observed growth rates are somewhat less than predicted, about 25 % less on average, but in view of the number of effects (viscosity, finite amplitude, etc.) which might contribute to a difference between the observations and predictions, the agreement is rather better than might be expected.

The observations are not sufficiently numerous to decide whether any variation with Reynolds number is present. The Reynolds number at the interface based on the velocity difference and the length scale $[2(\pi\kappa\tau)^{\frac{1}{2}}/Q]$ of the velocity transition region at the interface, at wave slopes of 0·2, ranges between 490 and 5000, which is higher than the values at which viscosity seems to play a significant part in the early growth of disturbances in homogeneous shear flows. At the

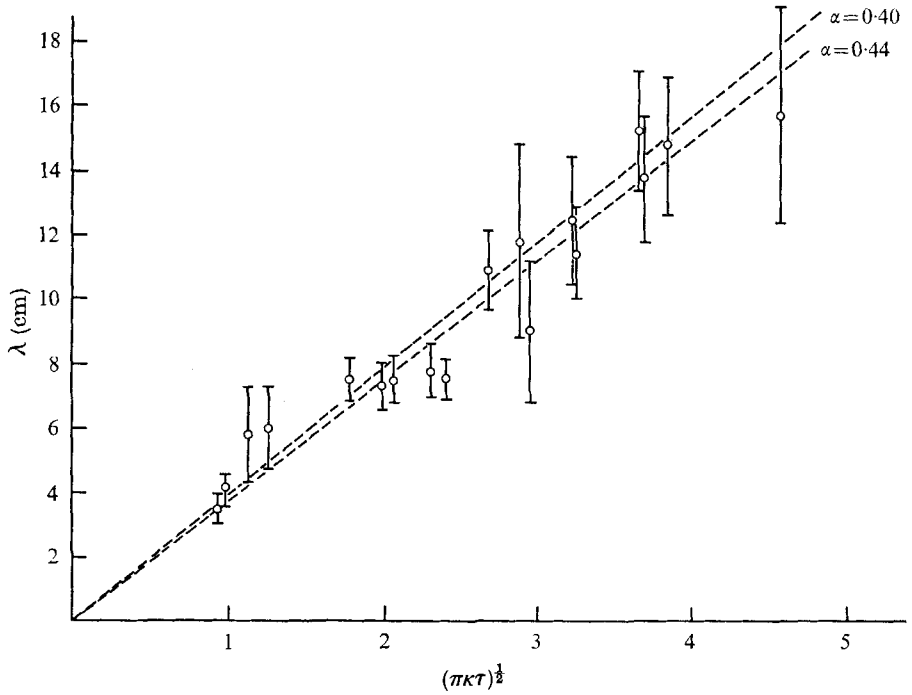

FIGURE 8. The variation of wavelength, λ, with the thickness of the interface $(\pi\kappa\tau)^{\frac{1}{2}}$. The vertical lines indicate the standard deviation of the observed points, and the dotted lines indicate the non-dimensional wave-numbers $\alpha = 0{\cdot}40$ and $\alpha = 0{\cdot}44$.

same wave slopes, 0·2, the Reynolds number at the walls of the tube, based on the largest velocity in the tube $(g\Delta t \sin\theta)$ and the length-scale, $(\pi\nu t)^{\frac{1}{2}}$, of the viscous boundary layer, ranges from 320 to 1400. The lower end of the range is such that Tollmien–Schlichting instabilities are not expected. At the upper end Tollmien–Schlichting instabilities are possible although their growth rate is not large. No sign of their presence in the experiments has been noticed.

The wavelength of the instability is not found to change during the growth from the smallest wave slopes which can be observed (about 0·01) up to the onset of turbulence or pairing (as described in I and shown in figure 5 in this paper) in which neighbouring rolls begin to wind around each other at wave slopes of order unity. It is therefore possible to select photographs of quite large amplitude disturbances for analysis of wavelengths. Figure 7 (plate 3) shows photographs of the disturbances which develop in a number of experiments in which the diffusion time τ has been varied. The wavelength λ of the instability increases as τ increases, and figure 8 shows the variation of λ with the length-scale

of the interface, $(\pi\kappa\tau)^{\frac{1}{2}}$. The mean wave-number, α non-dimensionalized with $(\pi\kappa\tau)^{\frac{1}{2}}$, in the experiments is 0·41 with standard deviation of 0·05. This is less than the critical wave-number, 0·48, calculated for the error function profiles and is also somewhat less than the wave-numbers near the computed curve of maximum growth rate. The small values of J when instability is observed suggest that a wave-number of 0·44 should be the largest. However, the other effects considered in § 2 tend to reduce the wave-number of the largest wave, and the observed value is well within the range which might be expected from the theoretical estimates. The large scatter in wave-numbers, indicated by the vertical lines of figure 7, has also been predicted. The theoretical results suggest that the instability found in the experiments made with very diffuse interfaces (the largest τ) may be affected by the presence of the tube boundaries, but the scatter in the observed wave-numbers makes it uncertain whether this is so.

3.3. *The growth to large amplitude*

The growth rates increase between wave slopes of 0·2 and 0·4 as the wave evolves into a spiral structure (see III), but between 0·4 and 1·2 (the slope at which the smooth outline of the spiral is first broken by irregular disturbances of scales small compared with the wavelength), the rate of change of wave amplitude with time is remarkably constant. Figure 9 shows the growth rates at wave slopes of 0·8. As in figure 6, the scatter of points is considerable. The growth rates are about half those measured at slopes of 0·2.

As the wave and the spiral structure grow, the phase difference between the crest and trough, initially 180° for the very small amplitude waves, decreases. The decrease appears to be quite irregular in the early stages, but between wave slopes of 0·4 and 1·2 the rate of change of phase is remarkably constant. At 0·4 the phase difference is about 90°, but when the first irregularities appear in the outline of the spiral structure the crest and trough are almost exactly in phase. We have thus a spiral structure which grows in total amplitude at a constant rate and in which the phase changes uniformly.

The fluid within the spiral when the outline is first broken has an approximately elliptical shape with the minor axis vertical, and the areas of these regions have been measured from the ciné film. If this fluid were spread along the tube the half thickness of the layer so formed would be about $1{\cdot}25(\pi\kappa\tau)^{\frac{1}{2}}$, with values nearer $(\pi\kappa\tau)^{\frac{1}{2}}$ for the longest waves observed and near $1{\cdot}75(\pi\kappa\tau)^{\frac{1}{2}}$ for the shortest. (The shorter wavelengths have generally rather larger wave-slopes (1·4) when the breakdown occurs, and it is probable that the tube boundaries affect the longer waves when their amplitude is large.) Since the density at a height $z = 1{\cdot}25(\pi\kappa\tau)^{\frac{1}{2}}$ is $\rho_0(1 - 0{\cdot}883\Delta)$ (from (3)), much of the fluid at the interface is involved in the spirals, and mixed as the spirals themselves become unstable.

The most regular spiral structures have been observed in the shallow (3 cm deep) tank used for the experiments described in I. Some attempts have been made to measure the distribution of angular velocity within the spirals in order to estimate the stability of the distribution, but these have not been very satisfactory. In growing to wave-slopes of about 1·2, the interface near the centre of the spiral has rotated through about 3π radians in the cases in which it

can still be distinguished. It is most frequently observed that the structure in the spirals becomes indistinct at quite an early stage in their growth and this is possibly the result of gravitational instabilities. If two inviscid fluids are superimposed with the heavier (ρ_2) above the lower (ρ_1) and with fractional density difference $\Delta = (\rho_2 - \rho_1)/(\rho_1 + \rho_2)$, the growth rate of unstable disturbances of wave-number k is $(gk\Delta)^{\frac{1}{2}}$ (Taylor 1950). If $k = 2\pi\,\mathrm{cm}^{-1}$ and $\Delta = 0{\cdot}08$, then the growth rate is about $22\,\mathrm{sec}^{-1}$ and in $\frac{1}{2}$ sec (a time typical of the growth of the spirals) the disturbance will have grown in magnitude by 6×10^4 times. Similar growth rates can be obtained if viscosity is included (see Chandrasekhar 1961,

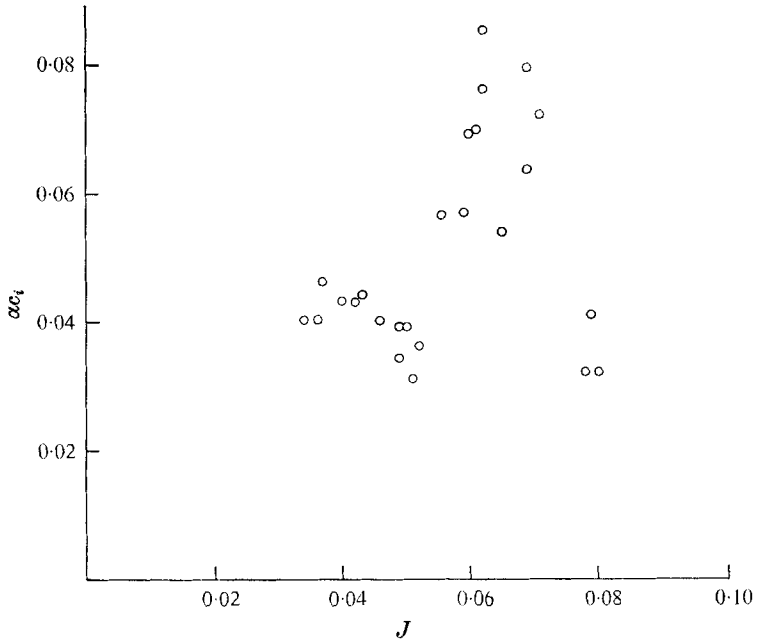

FIGURE 9. The observed non-dimensional growth rates, αc_i, as functions of the minimum Richardson number, J, when the slope of the disturbance is 0·8.

ch. 10). The edges of the spirals and the interface between them is frequently disturbed by an instability which resembles the initial instability but on a smaller scale, and small-scale spirals are formed.

Some experiments have been made with a number of layers, and figures 10–12 (plates 4–6) show the onset of instability for 3 layers, 5 layers and 7 layers respectively. The initial density distributions are given in the figure captions. In the case of the 3- and 5-layer experiments, instability is first seen to grow at the upper interface and the resulting disturbances move with about the mean speed of the fluid at that level, and only later is the lower fluid involved in the mixing. In both cases the instability occurs first at the interface where the density jump is greatest and therefore where the Richardson number is least. A variety of length scales can also be seen to be generated in this process. Some of the smaller spirals which grow on the larger (see, for example, figure 10(*h*)) may be the cause of the large reflexions from such structures observed by radar

in the clear atmosphere (see, for example, Hicks & Angell 1968; Browning & Watkins 1970). The 7-layer experiment, figure 12, has become unstable in a similar fashion to the 2-layer experiments, and the distortion of the bands of dye show clearly the way in which fluid is transported and redistributed in the spiral growth and the subsequent 'cats-eye' type pattern. The small columns of dyed fluid which are seen to emerge from the lower edge of the dyed band (figure 11 (f)) possibly result from an overshoot of gravitationally unstable fluid in the break-up of the spiral-like flow.

3.4. *The resulting turbulence*

The onset of small-scale irregularites in the smooth outline of the spiral pattern are first observed at wave-slopes between about 1·2 and 1·4, and these are followed by a transition which results in the production of a layer of mixed fluid bounded by an irregular boundary. This layer appears to be turbulent. If the tilt of the tube is maintained, the turbulent layer rapidly spreads to fill the whole depth of the tube. Some experiments have been made, however, in which the tube is tilted until instability just begins, and the tube is then rapidly returned to the horizontal position. Provided that the diffusion time is small, so that the interface is thin and the wavelength of the instability small, the resulting turbulent layer does not fill the tube, and it is possible to examine its growth and decay in conditions in which presence of the tube boundaries may not be significant. It is found that by shining the almost collimated beam of light from a slide projector through the tank on to a screen of tracing paper much of the fine structure within and at the boundaries of the turbulent layer is revealed. (This is a simple shadow-graph.)

A few experiments have been made with values of Δ equal to about 0·04, τ equal to about 25 min and, approximately, $\sin\theta = 0{\cdot}10$ during the time the tube is tilted. The experiments have not been repeated over a wider range of conditions since the influence of the tube boundaries is uncertain. Nevertheless they seem to be of sufficient interest to merit the inclusion of a general description at this stage. Figure 13 (plate 7) shows (in negative from the 16 mm colour ciné film) the development of the mixed layer, and figure 14 shows the variation of layer thickness with time measured from the onset of small-scale irregularities in the flow at wave slopes of about 1·3. The half thickness of the layer, D, has been non-dimensionalized with respect to the length $U_0^2/g\Delta$, where U_0 is the estimated fluid speed outside the layer when the tube is returned to the horizontal position; $U_0 = g\Delta t \sin\theta$, where t equals the time for which the tube was tilted. This non-dimensionalized thickness is equal to the layer Richardson number, R_{iL}. The time, T, has been non-dimensionalized with respect to $U_0/g\Delta$.

The tube becomes horizontal at, or about, $T = 0$. Thereafter the mixed layer grows at almost a constant rate with $dR_{iL}/dT = 0{\cdot}1$, until R_{iL} is about 0·32, when the rate decreases a little. The value $R_{iL} = 0{\cdot}40$ is reached at about $T = 5$, after which there is little further growth of the layer. The layer thickness is then about 6 cm and it thus fills a large proportion of the tube height (10 cm). During the early stages of growth the edge of the turbulent region is marked mainly by rounded billows (figure 13 (d)–(g)) which at first have a largest scale

similar to the scale of the spiral rolls; evidence of the roll-like structure is lost at about $R_{iL} = 0{\cdot}2$ and the scale of the billows is then reduced. A transition in the nature of the edge of the layer occurs at about $R_{iL} = 0{\cdot}37$, and instead of rounded billows a striated structure becomes more and more dominant (figure 13(*i*), (*j*)). The Reynolds number at the walls of the tube ($U_0(\pi t/\nu)^{\frac{1}{2}}$, where t is the time elapsed since the tube was first tilted) is equal to 1000 when T is about 8.

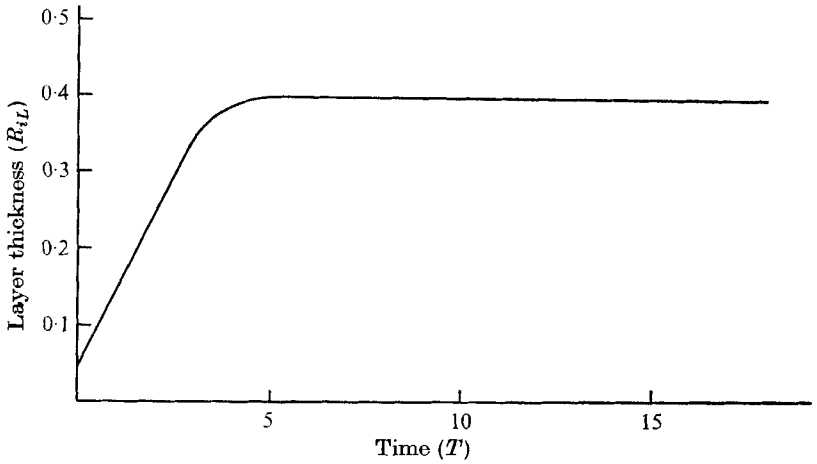

FIGURE 14. The variation of the non-dimensional thickness of the layer resulting from instability in the shear flow (or the layer Richardson number R_{iL}) with non-dimensional time T, at the values of Δ, τ and $\sin\theta$ given in §3.4.

At about $T = 10$ the boundary is almost entirely marked by lines and striations, and at about this time the first striations or layers within the turbulent layer are seen (figure 13(*k*)). Until this time there is little notable structure within the layer. What there is consists of rather round and indistinct shadows which move as if in a uniform shear. The striations within the layer become stronger and more numerous and completely dominate the structure at about $T = 16$. They are slightly inclined to the horizontal as shown in figure 13(*m*), (*n*). Their presence appears to indicate the collapse of the vertical motions in the turbulence and the establishment of a fine-scale density structure which moves with approximately uniform shear, U_0/D, in the layer. The inclination of the strong streaks (figure 13(*m*), (*n*)) is consistent with the assumption that they are the sheared remnants of individual rolls which in mixing have arrived at slightly different densities. The influence of the ends of the tube becomes apparent at about $T = 18$ and further unimpeded development cannot be followed. The construction of a larger tube may allow further detailed study of the turbulent layer and its collapse, and an investigation of energy exchanges in the turbulent motions.

4. Final remarks

We have discussed a simple experiment in which instability occurs in a stratified free-shear flow in which both the density and velocity profiles have an error function form. The agreement between observations and theory similar

to that first developed by Taylor (1931) and Goldstein (1931) suggests that the instability arises from the so-called Kelvin–Helmholtz instability. The growth of the instability from wave-slopes of 0·2 until the onset of the collapse of the resulting turbulence have been described in some detail.

The flow in the experiments and those which occur in nature are not steady. The reduction of the minimum Richardson number, J, to values well below the critical value necessary for instability in steady flows before instability becomes noticeable in the accelerating flows, is a remarkable feature of the experiments, and care should be taken to allow sufficient time for the growth of disturbances when making estimates of the conditions for instability in naturally occurring non-steady flows.

I am grateful for the assistance of several students who have helped to make the experiments during their university vacations, and to the many staff at N.I.O. who have helped in making the apparatus or in taking photographs. A film of these experiments and those reported in II is being made, and anyone interested in obtaining a copy should write to the author for details.

Appendix. The effect of viscosity on the accelerating flow

It was shown in I that the Laplace transform of the velocity in the tilted tube,

$$\bar{u}(z,s) = \int_0^\infty e^{-st}\, u(z,t)\, dt,$$

is given by

$$\bar{u} = A\sinh rz + B\cosh rz + C + \frac{g\sin\theta}{\mu s r}\int_0^z \rho(y)\sinh r(z-y)\, dy, \qquad \text{(A 1)}$$

where μ is the coefficient of viscosity, supposed constant, $\nu = \mu/\rho_0$, $r = (s/\nu)^{\frac{1}{2}}$ and A, B and C are functions of s to be determined from the boundary conditions and the condition

$$\int_{-\frac{1}{2}H}^{\frac{1}{2}H} \bar{u}\, dz = 0. \qquad \text{(A 2)}$$

(A factor $1/r$ was omitted from the last term in the form of (A 1) published in I.)

We are here concerned with the flow near $z = 0$, in the shear layer, and accordingly we let $\rho = \rho_0(1-\Delta f(z))$ and $u = g\Delta f(z)\, t\sin\theta$ at $z = \pm\frac{1}{2}H$ and assume that $\Delta \ll 1$, and $f(z) = -f(-z)$ is of order unity, as in § 2.1. This choice of u will remove the effects of the wall boundary layers when we take the limit $H \to \infty$. Imposing the conditions (A 2) and $\bar{u} = g\Delta f(\pm\frac{1}{2}H)/s^2$ at $z = \pm\frac{1}{2}H$ on (A 1) we find that

$$\bar{u} = \frac{g\Delta\sin\theta}{s^2\sinh(\frac{1}{2}rH)}\{[f(\tfrac{1}{2}H) + r\Psi(\tfrac{1}{2}H)]\sinh(rz) - r\Psi(z)\sinh(\tfrac{1}{2}rH)\} \qquad \text{(A 3)}$$

and

$$\frac{\partial\bar{u}}{\partial z} = \frac{g\Delta\sin\theta}{s^2\sinh(\frac{1}{2}rH)}\{rf(\tfrac{1}{2}H) + r^2\Psi(\tfrac{1}{2}H)\} \quad \text{at} \quad z = 0, \qquad \text{(A 4)}$$

where

$$\Psi(z) = \int_0^z f(y)\sinh r(z-y)\, dy.$$

If now

$$f(z) = \operatorname{erf}\beta z,$$

corresponding to the experimental conditions, we find that, on substitution,

$$\frac{\partial \bar{u}}{\partial z}(z=0) \to \frac{g\Delta \sin\theta}{s^2}\left(\frac{s}{\nu}\right)^{\frac{1}{2}}[1-\operatorname{erf}(r/2\beta)]\exp(s/4\nu\beta^2) \quad \text{as} \quad H \to \infty.$$

This expression may be inverted by using the tables of integral transform (Erdelyi *et al.* 1954, p. 267 (15)) and re-written using formula for the hypergeometric function (Abramowitz & Stegun 1965, p. 556; 15.1.13) to give in the limit $H \to \infty$

$$\frac{\partial u}{\partial z}(z=0) = \frac{4\beta g \Delta t \sin\theta}{\pi^{\frac{1}{2}}[1+(1+4\nu t\beta^2)^{\frac{1}{2}}]}.$$

Now the velocity gradient at $z = 0$ in an inviscid flow with density profile given by (3) is

$$\frac{\partial u}{\partial z}(z=0) = \frac{g\Delta t \sin\theta}{(\pi\kappa\tau)^{\frac{1}{2}}},$$

and so, putting $\beta = 1/2(\kappa\tau)^{\frac{1}{2}}$, we find that the ratio of the shear in a viscous flow to that in an inviscid flow is

$$Q = \frac{2}{\{1+[1+(4/\pi)(\nu t/\kappa\tau)]^{\frac{1}{2}}\}}. \tag{A 5}$$

REFERENCES

Abramowitz, M. & Stegun, I. A. 1965 *Handbook of Mathematical Functions.* New York: Dover.

Betchov, R. & Szewczyk, A. B. 1963 *Phys. Fluids*, **6**, 1391.

Browning, K. A. & Watkins, C. D. 1970 *Nature, Lond.* **227**, 260.

Chandrasekhar, S. 1961 *Hydrodynamic and Hydromagnetic Stability.* Oxford: Clarendon.

Drazin, P. G. 1970 *J. Fluid Mech.* **42**, 321.

Drazin, P. G. & Howard, L. N. 1966 *Adv. Applied Mech.* **9**, 1.

Erdelyi, A., Magnus, W., Oberhettinger, F. & Tricomi, F. G. 1954 *Tables of Integral Transforms*, vol. I. Bateman Manuscript Project. New York: McGraw-Hill.

Esch, R. 1957 *J. Fluid Mech.* **3**, 289.

Freymuth, P. 1966 *J. Fluid Mech.* **25**, 683.

Goldstein, S. 1931 *Proc. Roy. Soc.* A **132**, 524.

Hazel, P. 1970 Ph.D. thesis, University of Cambridge.

Hicks, J. J. & Angell, J. K. 1968 *J. Appl. Meteorol.* **7**, 114.

Holmboe, J. 1962 *Geofys. Publr.* **24**, 67.

Miles, J. W. 1963 *J. Fluid Mech.* **16**, 209.

Mowbray, D. E. 1966 *J. Fluid Mech.* **27**, 595.

Scotti, R. S. & Corcos, G. M. 1969 *Radio Sci.* **4**, 1309.

Taylor, G. I. 1931 *Proc. Roy. Soc.* A **132**, 499.

Taylor, G. I. 1950 *Proc. Roy. Soc.* A **201**, 192.

Thorpe, S. A. 1968 *J. Fluid Mech.* **32**, 693.

Thorpe, S. A. 1969*a* *J. Fluid Mech.* **39**, 25.

Thorpe, S. A. 1969*b* *Radio Sci.* **4**, 1327.

Thorpe, S. A. 1969*c* *J. Fluid Mech.* **36**, 673.

Woods, J. D. 1968 *J. Fluid Mech.* **32**, 791.

Yih, C-S. 1955 *Quart. Appl. Math.* **12**, 434.

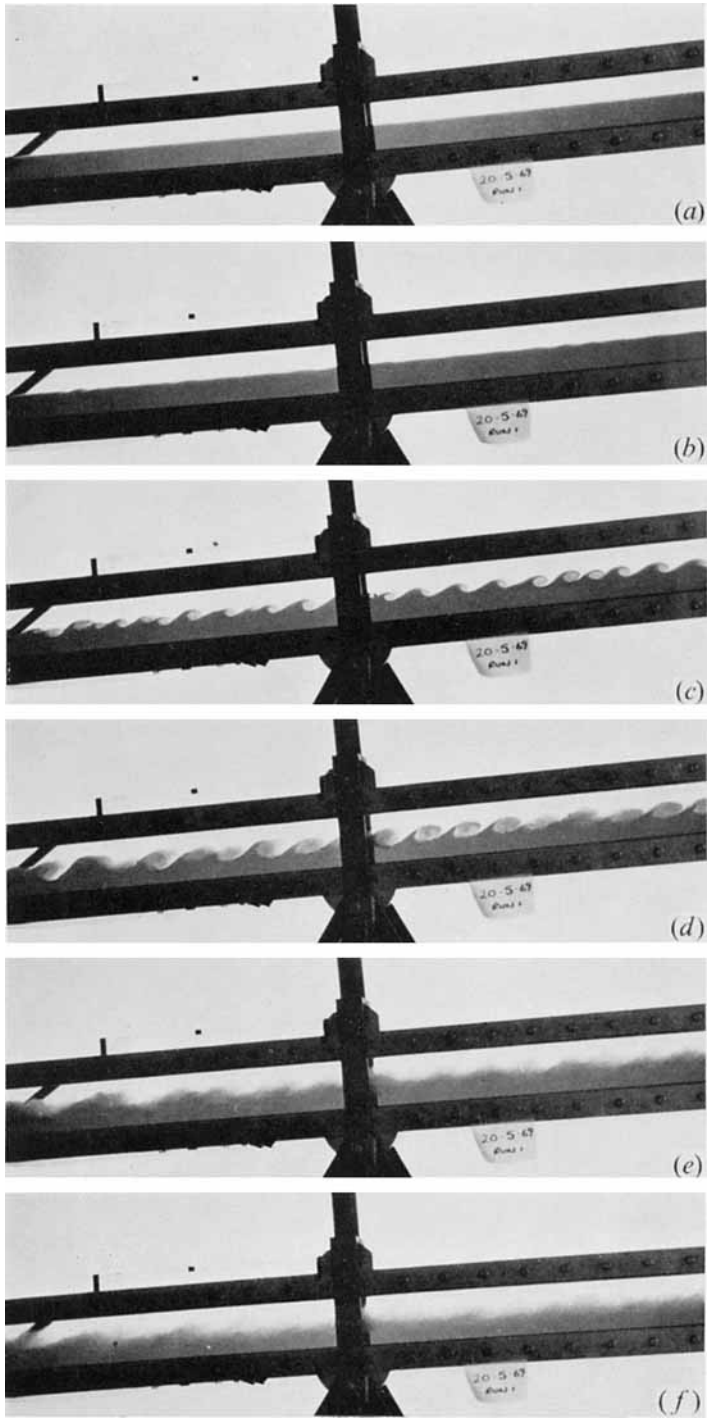

FIGURE 1. The growth of the instability at the interface of layers of water and brine coloured with potassium permanganate of equal depth and fractional density difference $\Delta = 7{\cdot}95 \times 10^{-2}$ g/cc. Diffusion has occurred for a time $\tau = 30$ min before the tube was tilted through 4·4°. The first photograph is taken at 3·35 sec after the tube has been tilted and the time interval between successive frames is 0·35 sec. The rule is 45 cm long. The flow in this and other photographs, except for that of figure 13, is to the right at the top of the tube and to the left at the bottom.

THORPE

(*Facing p.* 320)

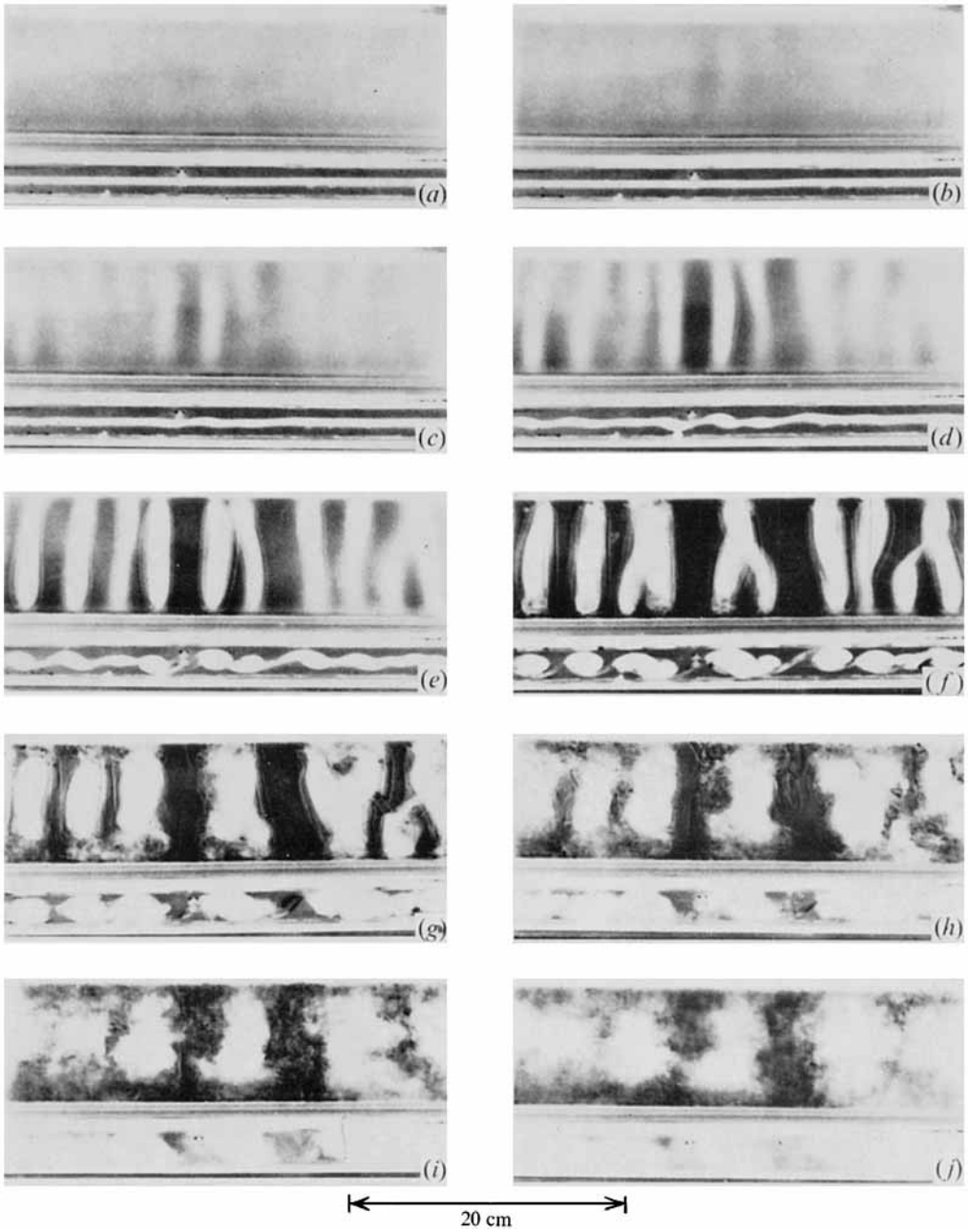

FIGURE 5. Instability at the interface between water and brine with $\Delta = 2{\cdot}90 \times 10^{-2}$ g/cc having a layer of dye at the interface. The photographs are taken from a 16 mm ciné film and are in negative so that the dye appears white. The upper part of each shows the plan view as seen through a mirror arranged at 45° to the horizontal and the lower part is a direct view. The tube has an internal cross-section of 3×10 cm. The first photograph is taken at 2·50 sec after tube has been tilted through 8·2°, and subsequent photographs are taken at 0·20 sec intervals.

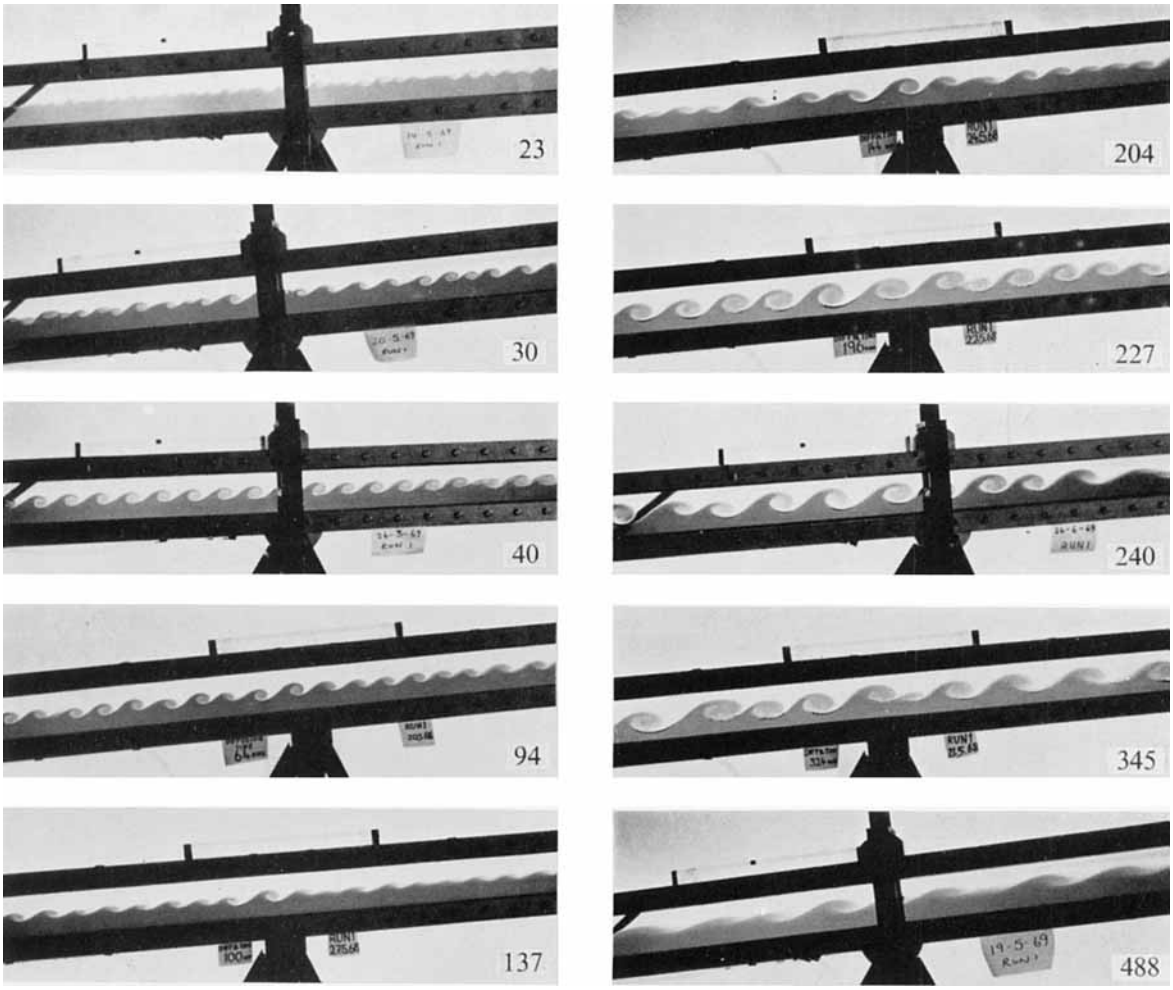

FIGURE 7. The variation of wavelength with diffusion time. The corrected diffusion time of each experiment in minutes is shown on the right. (The other labels are for use in identifying different experiments.) The rule is 45 cm long.

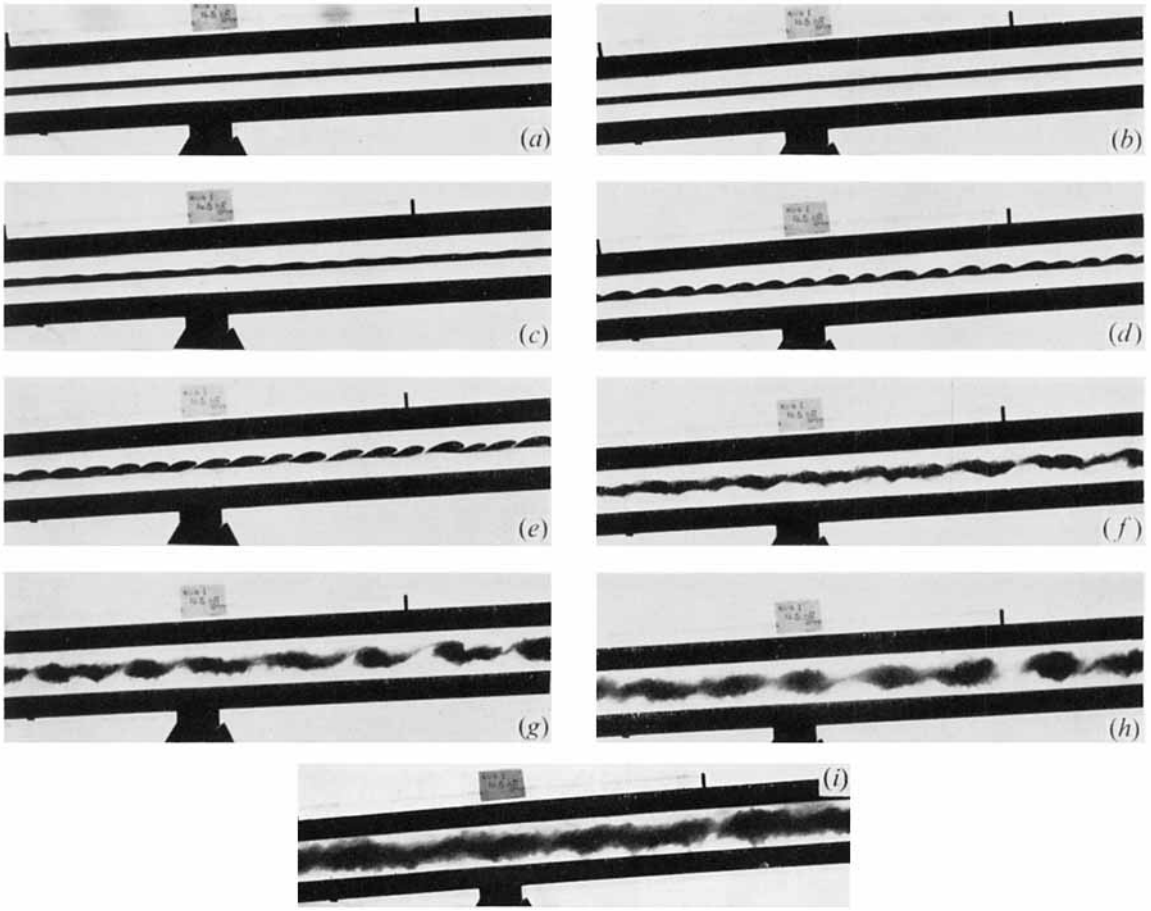

FIGURE 10. Instability in a three-layer experiment with densities 1·000, 1·092 and 1·172 g/cc, the central dyed layer having an initial thickness of 1·3 cm. Diffusion between the layers lasted for about 40 min before the tube was tilted through 5·6°. The first photograph was taken after 3·87 sec and those following at intervals of 0·44 sec.

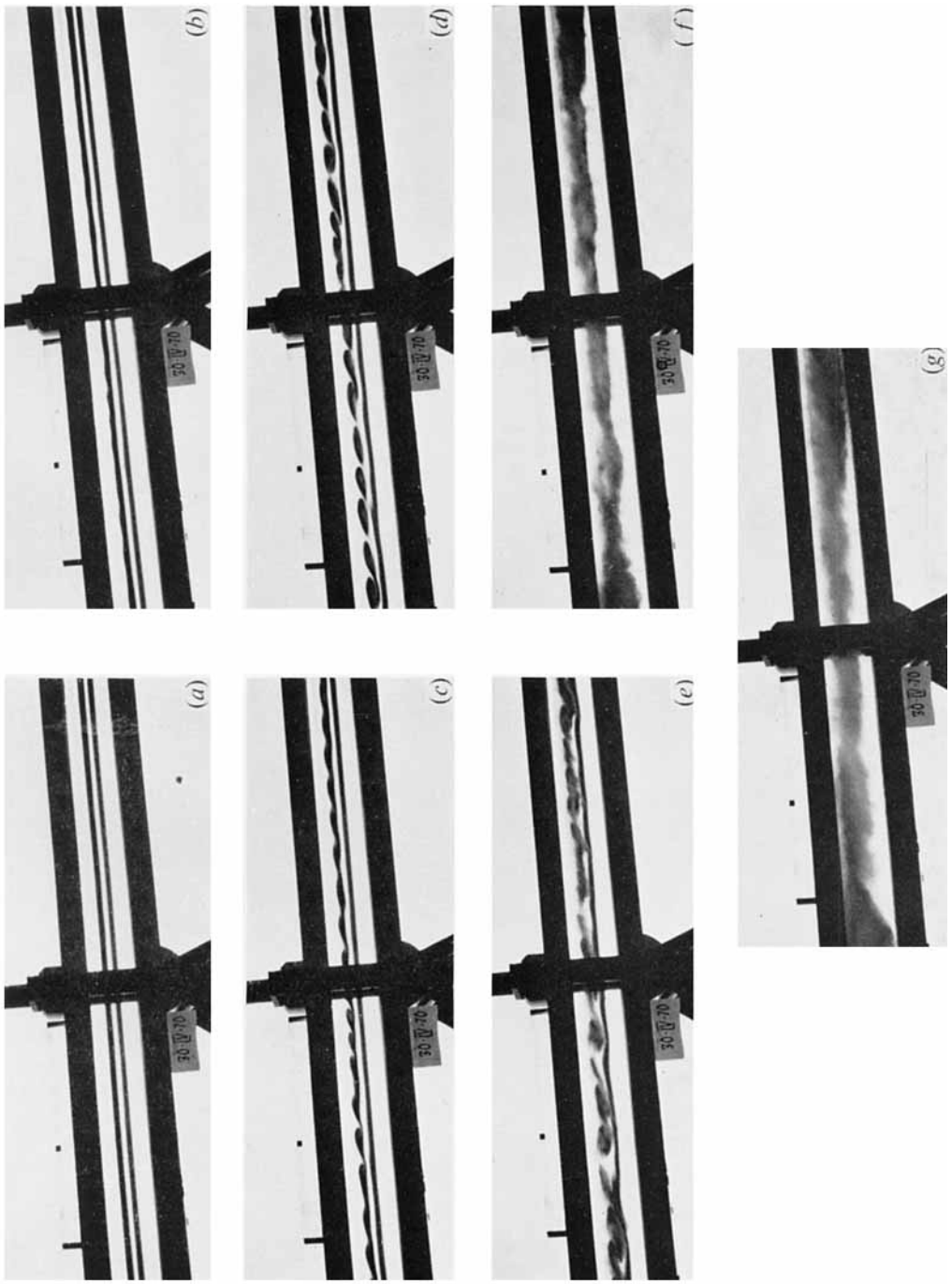

FIGURE 11. Instability in a five-layer experiment with densities 1·001, 1·046, 1·085, 1·126 and 1·164 g/cc, the three middle layers having initial depths of 1·02 cm. Diffusion between the layers lasted for about 25 min before the tube was tilted through 5·6°. The first photograph was taken after 5·13 sec and those following at intervals of 0·42 sec.

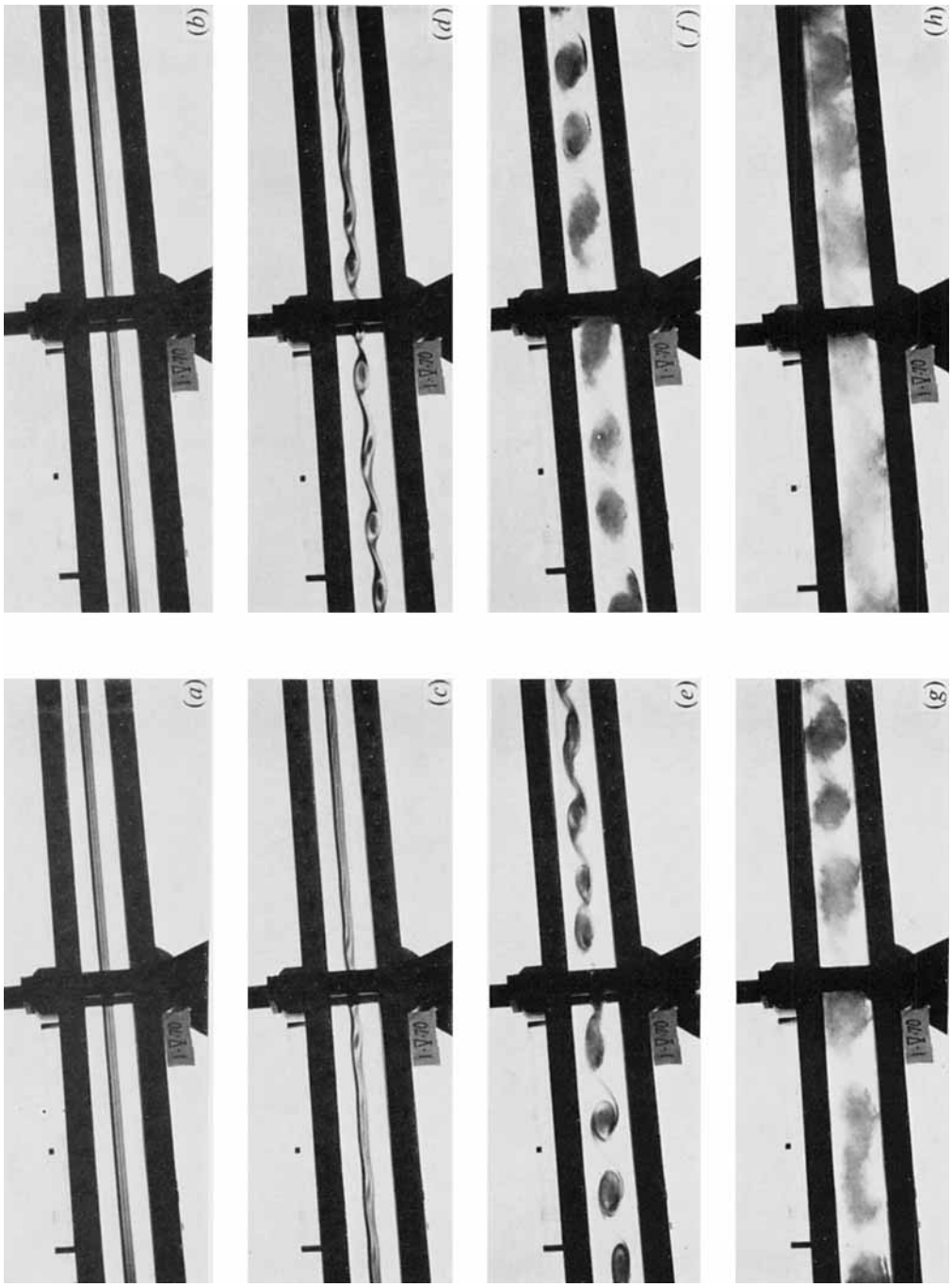

FIGURE 12. Instability in a seven-layer experiment with densities 1·004, 1·035, 1·044, 1·090, 1·135, 1·152 and 1·181 g/cc, the middle five layers having each an initial thickness of 0·41 cm. Diffusion between the layers lasted for about 20 min before the tube was tilted through 5·6°. The first photograph was taken after 3·28 sec and those following at intervals of 0·36 sec.

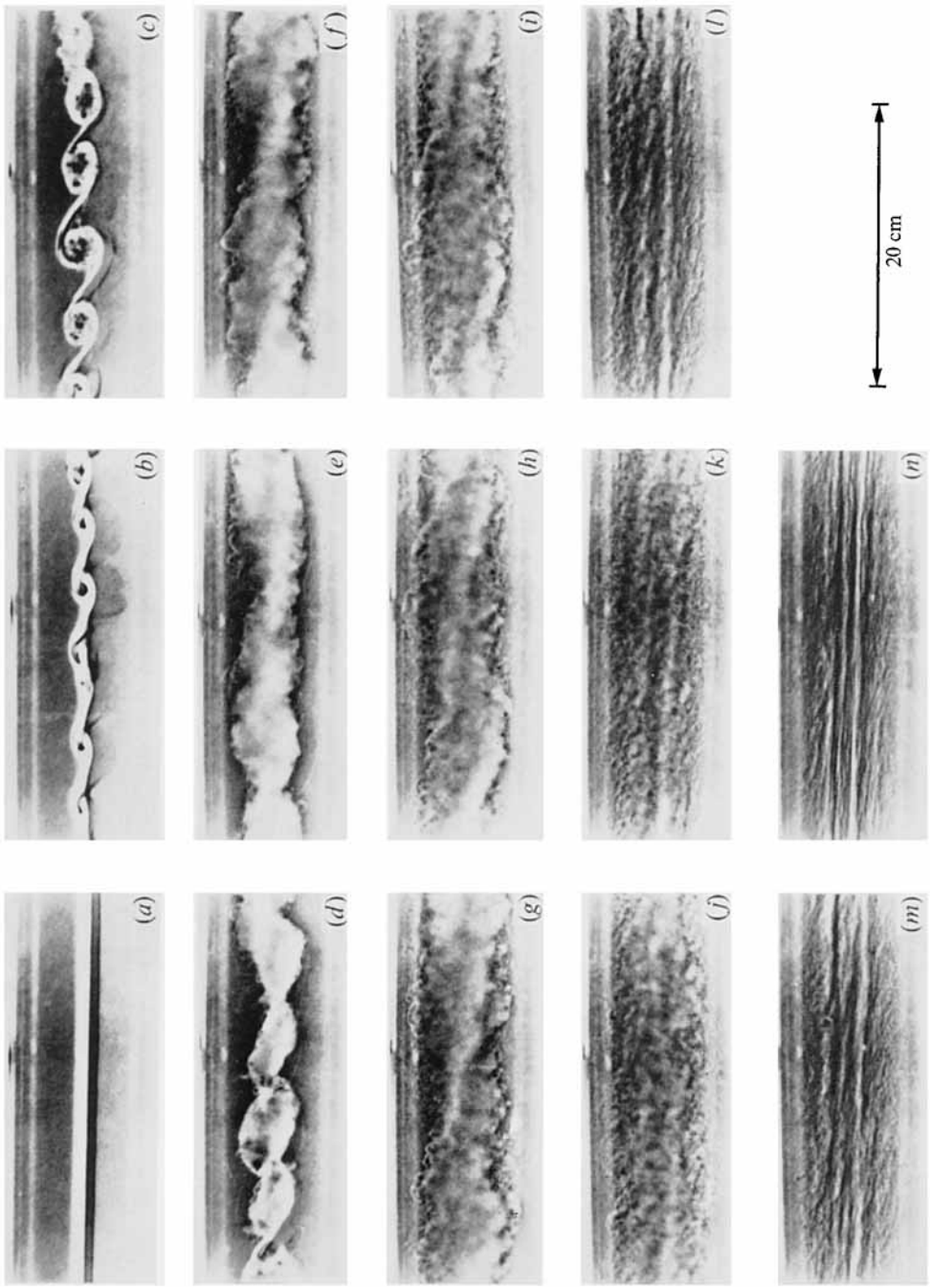

FIGURE 13. The turbulent layer resulting from instability. These photographs are taken from 16 mm ciné film of a shadow-graph of the spreading layer, and are here shown in negative. The fractional density difference, $\Delta = 3{\cdot}08 \times 10^{-2}$ g/cc; $\tau = 20$ min approximately; $\theta = 5{\cdot}6°$. The time for which the tube was tilted from the horizontal position is 5·10 sec and the photographs were taken at the following times after the tube was first tilted away from the horizontal. (*a*) 3·85 sec. The light band is at the position of the interface. The flow is to the left in the upper part of the tube, to the right below the interface. (*b*) 4·82 sec (the beginning of instability). (*c*) 5·20 sec (just after the tube is returned to the horizontal). (*d*) 5·60 sec. (*e*) 5·90 sec (the structure of the rolls is no longer visible in the shape of the boundary). (*f*) 6·28 sec. (*g*) 6·67 sec. (*h*) 7·05 sec. (*i*) 7·44 sec (striations have appeared at the edge of the layer; the layer thickness does not increase much after this time). (*j*) 8·58 sec. (*k*) 9·75 sec (the boundary is completely striated, and bands are beginning to form in the layer). (*l*) 10·90 sec. (*m*) 12·05 sec. (*n*) 14·35 sec.